Supporting Information

Nanozymes with Controllable Inhibition Modes Assist Primary Antithyroid Drug Screening

Lu Dong, Jiajun Li, Xiaolei Sun, Wei Zhang, Nana Guo, Yiming Zhang, Lijun Hu, Chengjie Chen, Lei Jiao and Yanling Zhai**

Institute of Molecular Metrology, College of Chemistry and Chemical Engineering, Qingdao University, Qingdao, 266071, P. R. China

E-mail: jiaolei@qdu.edu.cn; zhaiyanling@qdu.edu.cn

1. Experimental section

Instruments

Transmission electron microscopy (TEM) and high-resolution transmission electron microscopy (HRTEM) images were taken using a FEI Talos F200X G2 transmission electron microscope. X-ray photoelectron spectroscopy (XPS) spectra were acquired on a Thermo Scientific K-Alpha electron spectrometer. Crystal structures of samples were examined by X-ray diffraction (XRD) (Rigaku Smart Lab SE). Fourier transform infrared spectroscopy (FT-IR) measurements were performed on an IRTracer-100. All nanozyme kinetics data and UV-vis spectra were obtained by a multimode reader (Tecan Spark, Switzerland).

Materials

Chloroplatinic acid (H_2PtCl_6•$6H_2O$) glucosamine hydrochloride, D-(+)-Glucose monohydrate, horseradish peroxidase (HRP), methimazole (MMI), propylthiouracil (PTU), methyl-thiouracil (MTU), and carbimazole (CBZ) were purchased from Shanghai Aladdin Biochemical Technology Co., Ltd. Sodium acetate (NaAc), 3,3',5,5'-tetramethylbenzidine (TMB) and zinc chloride ($ZnCl_2$) were obtained from Shanghai Maclin Biochemical Technology Co., Ltd. LuDOX(R)TM-40 colloidal silica was purchased from Sigma-Aldrich. Hydrogen peroxide (H_2O_2) was purchased from Sinopharm Chemical Reagent Co., Ltd.

Synthesis of Pt_{NP}/NC

A homogeneous aqueous mixture containing $ZnCl_2$ (2 mmol), D-glucosamine hydrochloride (10 mmol), colloidal SiO_2 (5 mL) and H_2O (10 mL) was stirred for 10 minutes and subsequently lyophilized. The resulting powder was annealed in N_2 at 900 °C for 2 h (heating rate: 5 °C min^{-1}). The black product was immersed in 10% HF for 24 h to remove silica, affording nitrogen-doped carbon (NC). An aqueous suspension of NC (100 mg in 100 mL H_2O) was treated dropwise with H_2PtCl_6 (200 μL, 100 mM) under

stirring for 12 h. After centrifugation, washing and drying, the solid was reduced under Ar/H_2 (5%) at 900 ℃ to convert the adsorbed Pt ions into Pt_{NPs}, yielding Pt_{NP}/NC.C was prepared by the same protocol except that D-glucosamine hydrochloride was replaced with D-glucose. Pt_{NP}/C was obtained analogously by substituting NC with the as-prepared C.

Evaluation of the H_2O_2 kinetics

First, as for the kinetic data towards H_2O_2, 10 μL of nanozymes were added into the mixture, including TMB (100 μL, 1 mM), HAc–NaAc (100 μL, 0.1 M, pH 3.0), and different concentrations of H_2O_2 (100 μL). Kinetic data were obtained and fitted by the nonlinear regression following the Michaelis-Menten Equation 1:

$$\frac{1}{v} = \frac{K_m}{V_{max}[s]} + \frac{1}{V_{max}}$$

Where V is the initial velocity, [S] is the concentration of the substrate, K_m is the Michaelis–Menten constant, and V_{max} is the maximal reaction velocity.

Cyclic experiment

First, as for the cyclic experiment towards HRP, 100 μL of HRP (5 μg mL^{-1}) was added into the centrifuge tube with HAC–NaAc (1 mL, 0.1 M, pH 3.0) and was set up for high-speed centrifugation operation to remove the supernatant. Each centrifugation is considered to be a cycle, while the blank control group is also centrifuged to avoid material loss during the operation. After centrifugation, the buffer solution was added for the performance test.

Inhibitory effects of antithyroid drugs on the POD-like activity of Pt_{NP}/NC

The inhibitory effects of MMI on the POD-like activity of Pt_{NP}/NC were investigated by measuring the residual activity. The initial velocities of H_2O_2 reduction varying with Pt_{NP}/NC concentration were gauged by changing the concentrations of Pt_{NP}/NC from 0 to 20 μg mL^{-1} while maintaining the H_2O_2 concentration

at 100 mM. The same procedures were executed at MMI concentration (0.05 mM) to investigate the effect of MMI. The steady-state kinetics of Pt_{NP}/NC concerning H_2O_2 with MMI were studied by varying the H_2O_2 concentration while keeping the concentrations of MMI and Pt_{NP}/NC fixed. Lineweaver-Burk curves were used to calculate the Michaelis constant (K_m^I) and maximum reaction velocity (V_m^I) at different concentrations of antithyroid drugs. The Michaelis-Menten equation of the mixed-inhibition system could be expressed by Equation 2:

$$\frac{1}{V} = \frac{K_m}{V_m} \times \frac{1}{S}(1 + [I]/K_i) + \frac{1}{V_m}(1+[I]/K_i') \quad (2)$$

K^I_m, V^I_m and $[I]$ could be described as $\frac{K_m^I}{V_m^I} = \frac{K_m}{V_m}(1 + [I]/K_i)$, and $\frac{1}{V_m^I} = \frac{1}{V_m}(1+[I]/K_i')$, $[I]$ referred to the concentration of MMI. The slope of curves $\frac{K_m^I}{V_m^I} \sim [I]$ and $\frac{1}{V_m^I} \sim [I]$ were $\frac{K_m}{V_m K_i}$ and $\frac{1}{V_m K_i'}$ respectively. Therefore, we could derive K_i and K_i' by the secondary plotting method.

2. Supplementary Figures

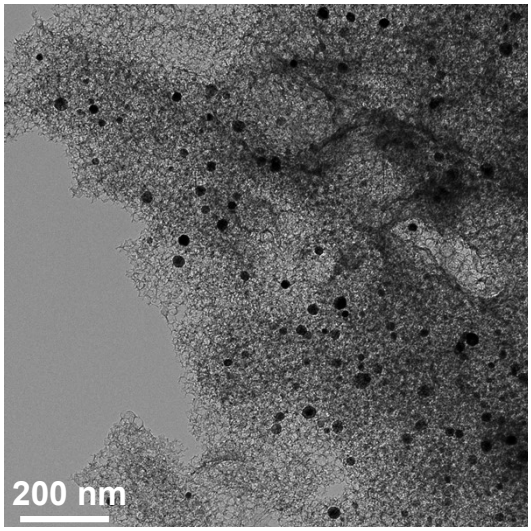

Figure S1. TEM of Pt_{NP}/NC.

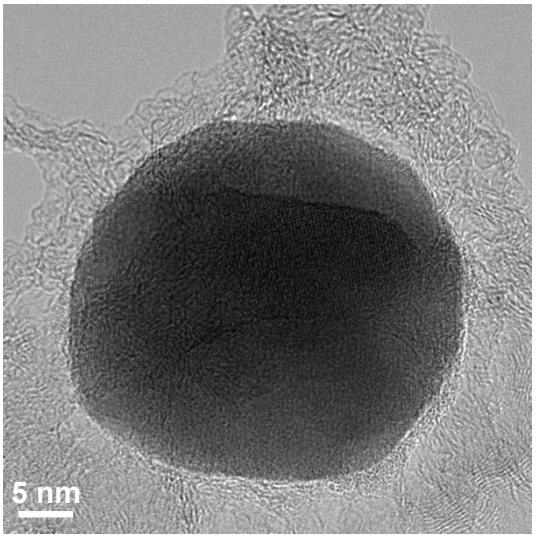

Figure S2. HRTEM images of Pt_{NP}/NC.

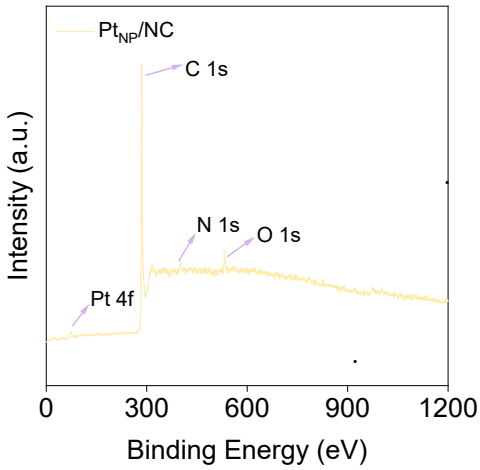

Figure S3. The survey XPS spectra of Pt_{NP}/NC.

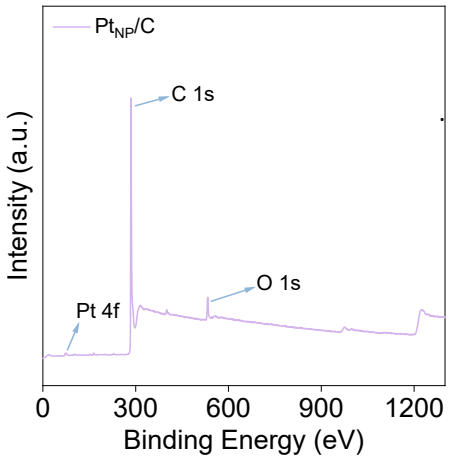

Figure S4. The survey XPS spectra of Pt_{NP}/C.

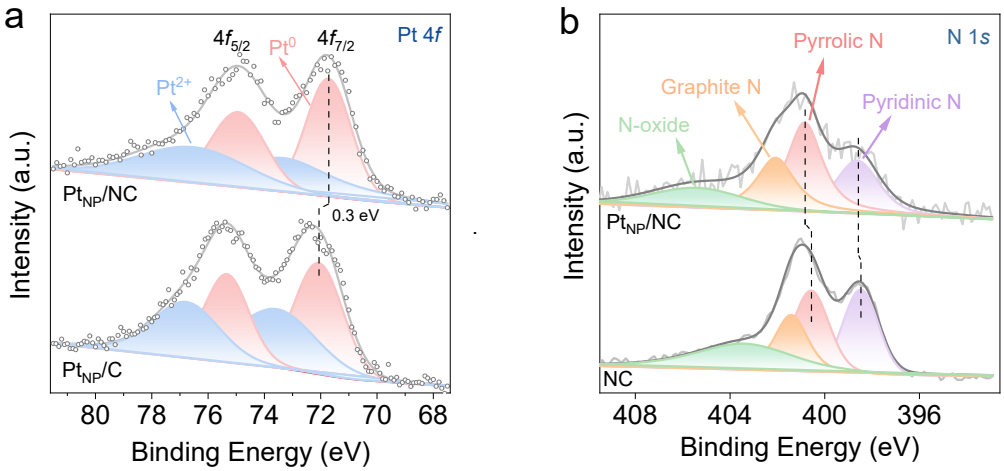

Figure S5 High-resolution XPS spectra of (a) Pt 4f, and (b) N 1s.

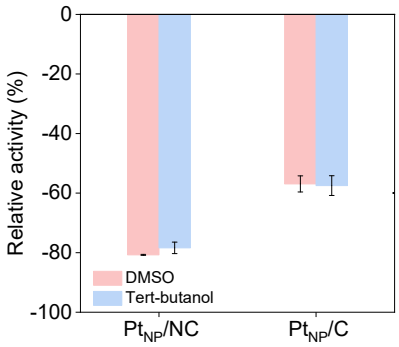

Figure S6. Absorbance inhibition degree of Pt_{NP}/NC and Pt_{NP}/C when DMSO and Ter-Butanol were used as intermediates quench agent.

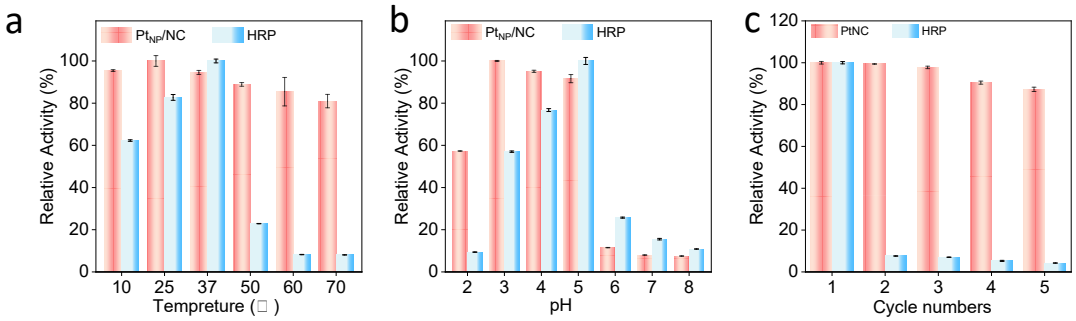

Figure S7. (a) Temperature-dependent and (b) pH activities for Pt_{NP}/NC nanozymes. (c) Absorbance values of TMB catalyzed by Pt_{NP}/NC and HRP for five cycles.

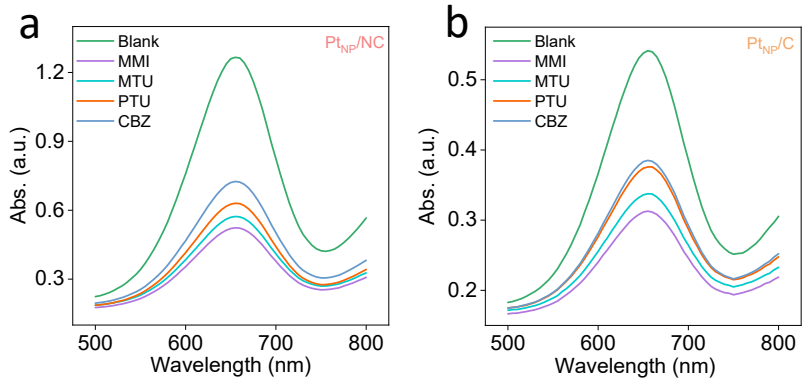

Figure S8. Absorption curves of Pt_{NP}/NC and Pt_{NP}/C with different antithyroid drugs (MMI, MTU, PTU and CBZ).

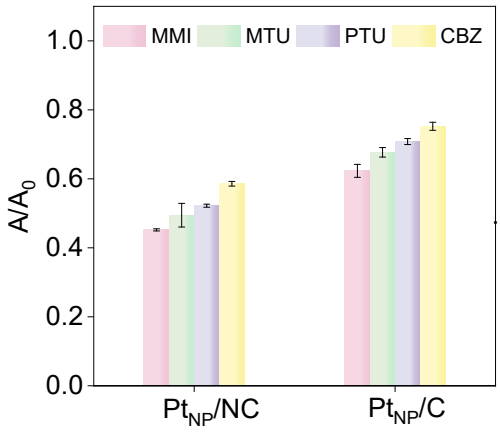

Figure S9. Colorimetric response patterns A/A_0 of sensor arrays toward four kinds of antithyroid drugs, where A signifies the absorbance in the presence of antithyroid drugs, and A_0 denotes the absorbance in their absence.

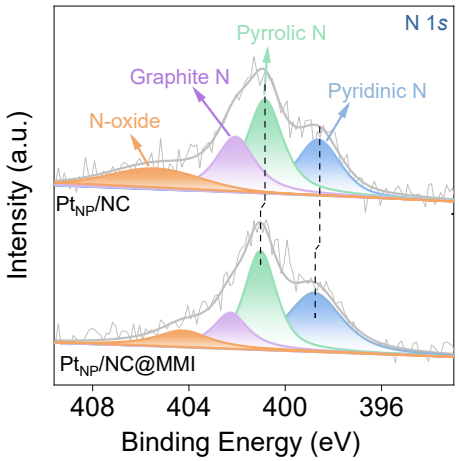

Figure S10. N 1s XPS spectra of Pt_{NP}/NC and MMI-combined Pt_{NP}/NC.

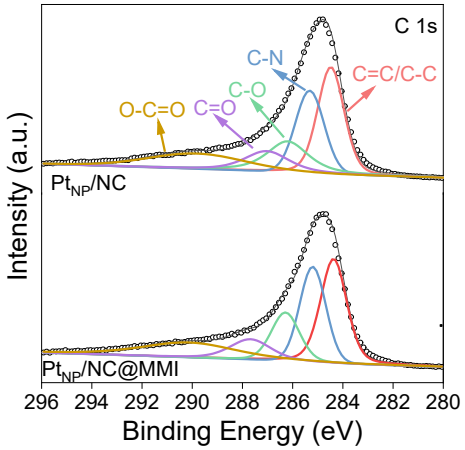

Figure S11. C 1s XPS spectra of Pt_{NP}/NC and MMI-combined Pt_{NP}/NC.

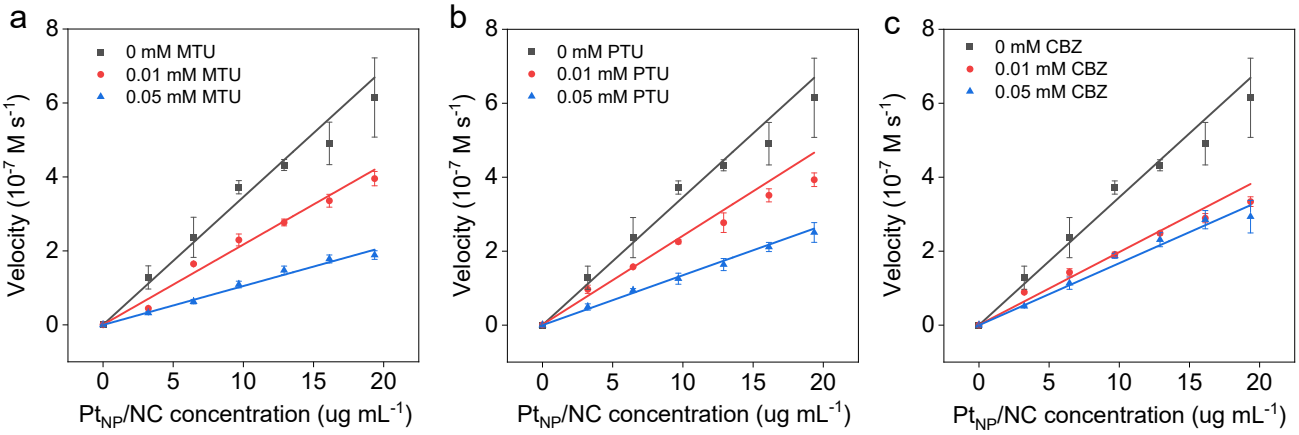

Figure S12. Pt_{NP}/NC at different MTU, PTU, and CBZ concentrations, respectively.

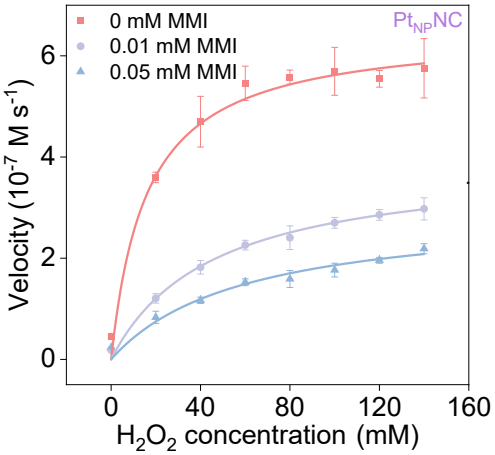

Figure S13. Michaelis−Menten curves of H_2O_2 activation by Pt_{NP}/NC at different MMI concentrations.

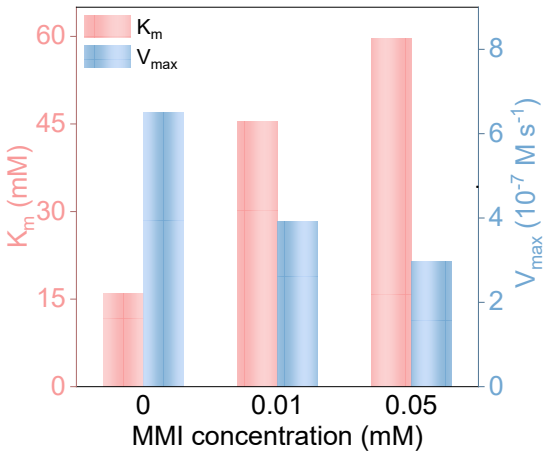

Figure S14. The K_m^I and V_{max}^I values of Pt_{NP}/NC in the presence of varying MMI concentrations.

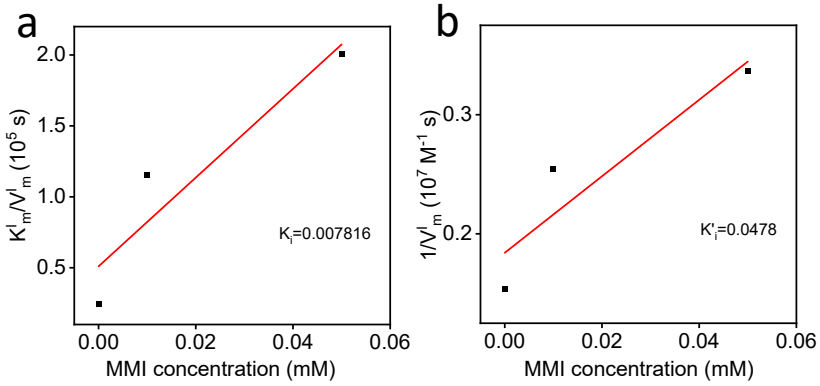

Figure S15. (a) Slopes ($1/V_m^I$) and (b) intercepts ($1/V_m^I$) of Lineweaver-Burk plots of Pt_{NP}/NC for H_2O_2 at different MMI concentrations.

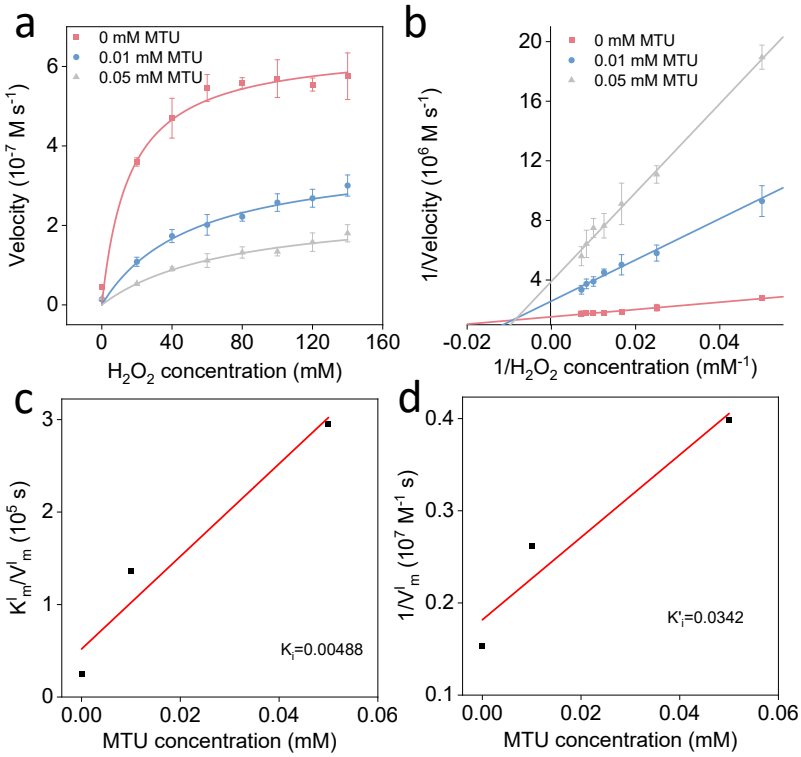

Figure S16. (a) Michaelis−Menten curves and (b) Lineweaver−Burk plots of H_2O_2 activation by Pt_{NP}/NC at different MTU concentrations. (c) slopes ($1/V_m^I$), and (d) intercepts ($1/V_m^I$) of Lineweaver-Burk plots of Pt_{NP}/NC for H_2O_2 at different MTU concentrations.

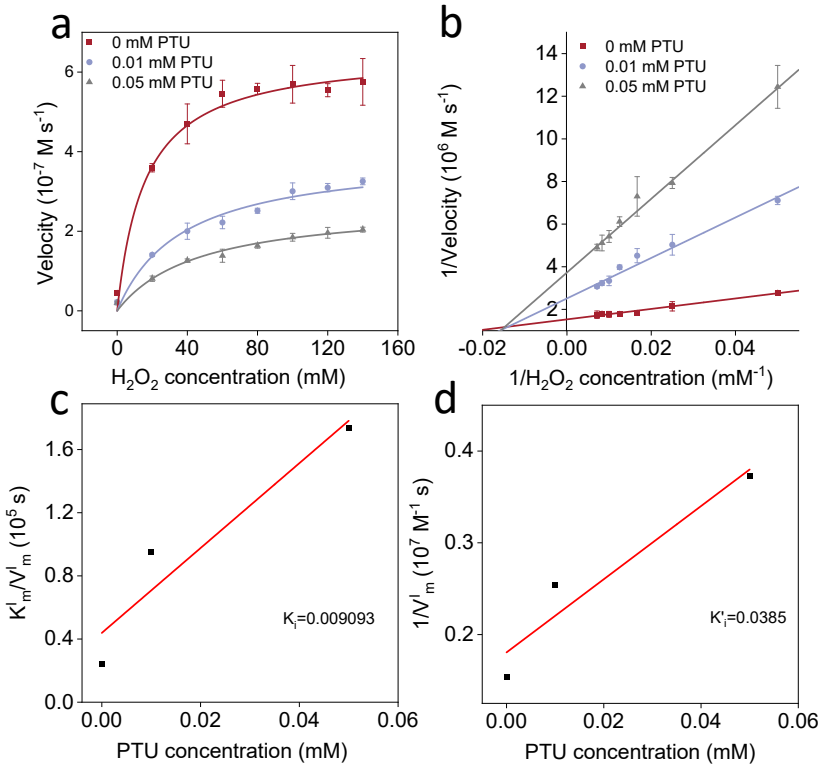

Figure S17. (a) Michaelis−Menten curves and (b) Lineweaver−Burk plots of H_2O_2 activation by Pt_{NP}/NC at different PTU concentrations. (c) slopes ($1/V_m^I$), and (d) intercepts ($1/V_m^I$) of Lineweaver-Burk plots of Pt_{NP}/NC for H_2O_2 at different PTU concentrations.

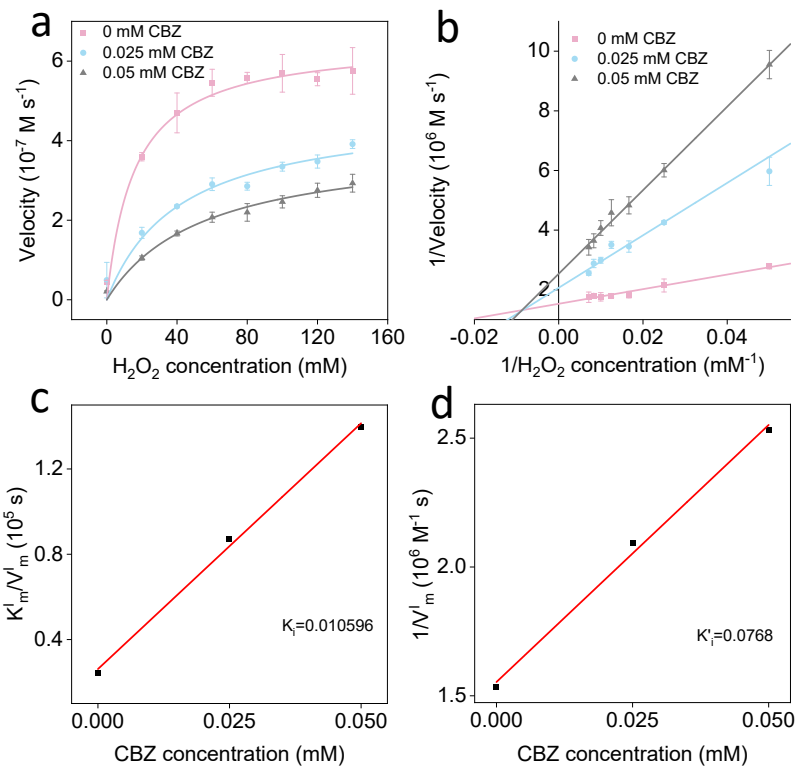

Figure S18. (a) Michaelis−Menten curves and (b) Lineweaver−Burk plots of H_2O_2 activation by Pt_{NP}/NC at different CBZ concentrations. (c) slopes ($1/V_m^I$), and (d) intercepts ($1/V_m^I$) of Lineweaver-Burk plots of Pt_{NP}/NC for H_2O_2 at different CBZ concentrations.

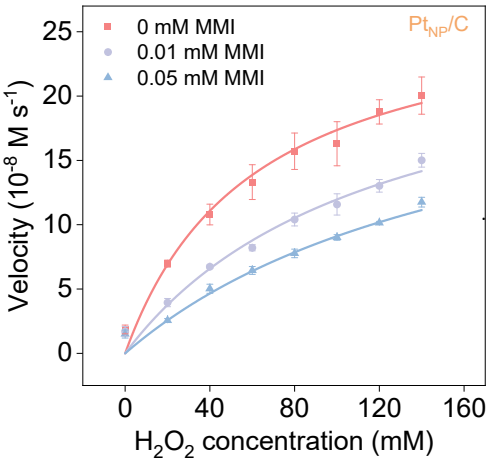

Figure S19. Michaelis−Menten curves of H_2O_2 activation by Pt_{NP}/C at different MMI concentrations.

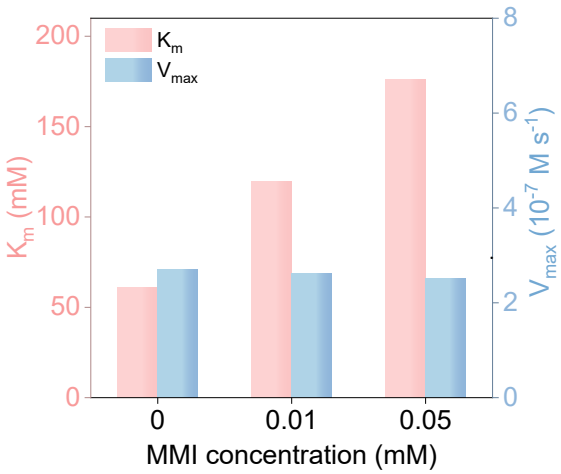

Figure S20. The K_m^I and V_{max}^I values of Pt_{NP}/NC in the presence of varying MMI concentrations.

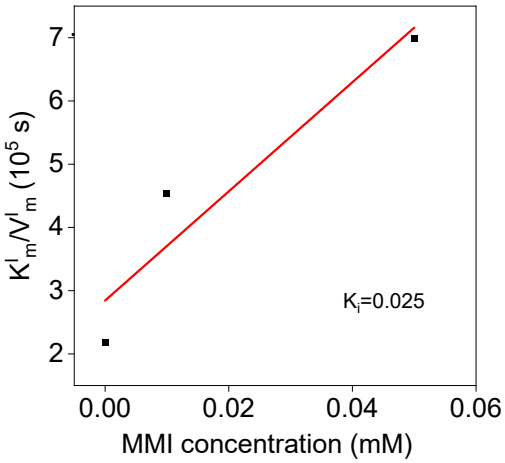

Figure S21. Slopes ($1/V_m^I$) of Lineweaver-Burk plots of Pt_{NP}/C for H_2O_2 at different MMI concentrations.

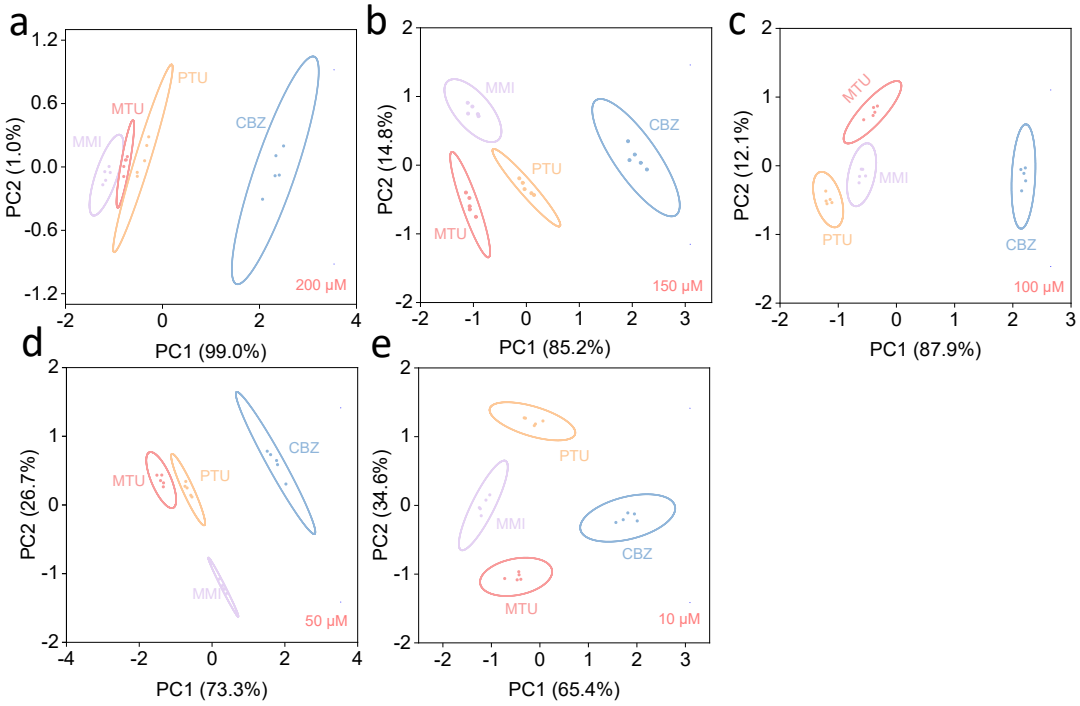

Figure S22. (a) 2D canonical score plots for the first two colorimetric response patterns A/A_0 factors towards 200 μM, (b) 150 μM, (c) 100 μM, (d) 50 μM, and (e) 10 μM.

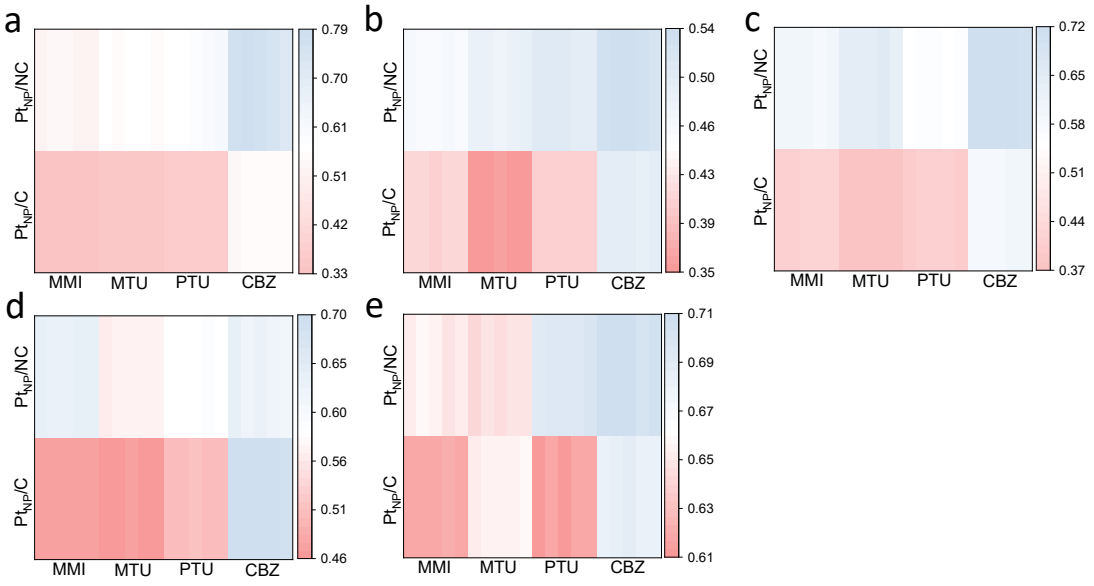

Figure S23. (a) The heat map originated from the absorbance changes A/A_0 of the sensor array against four kinds of antithyroid drugs at 200 μM, (b) 150 μM, (c) 100 μM, (d) 50 μM, and (e) 10 μM.

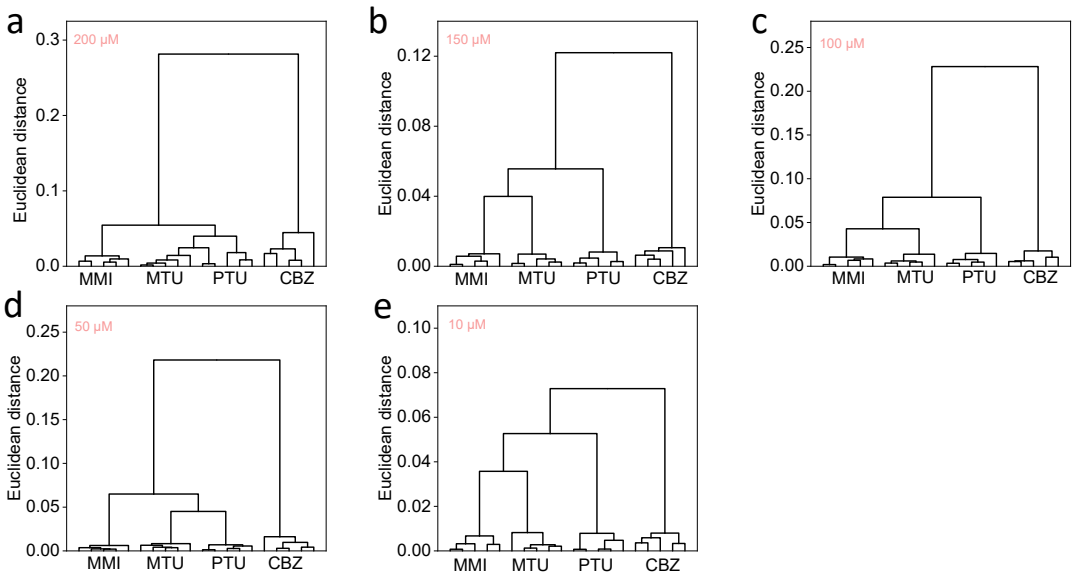

Figure S24. (a) Hierarchical cluster analysis of the absorbance changes A/A_0 of the sensor array against four kinds of antithyroid drugs at 200 μM, (b) 150 μM, (c) 100 μM, (d) 50 μM, and (e) 10 μM.

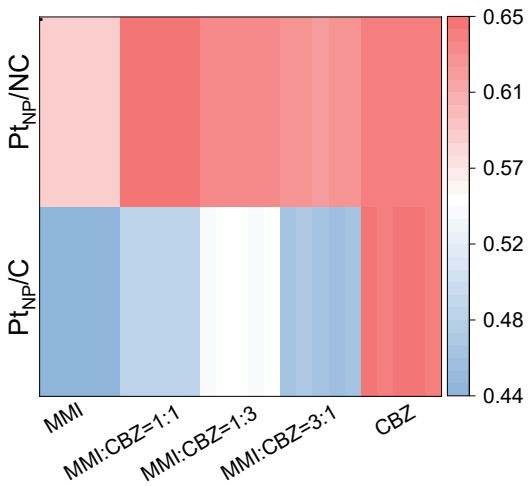

Figure S25. Heat map of the sensor array in response to a mixture of MMI and CBZ in different proportions.

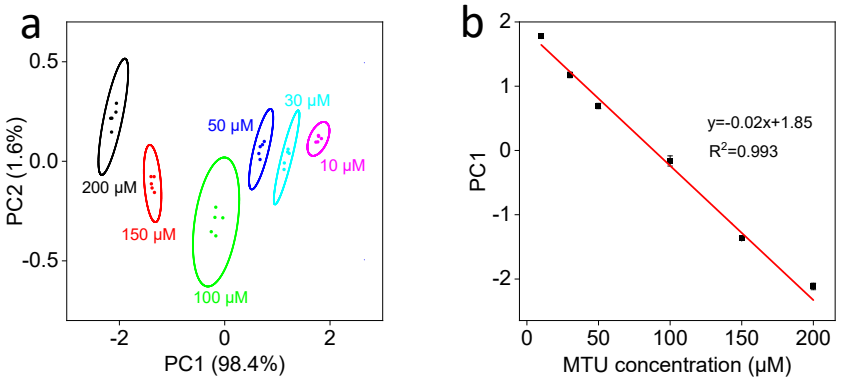

Figure S26. PCA canonical score plots and the linear calibration plots for the discrimination of different concentrations of MTU.

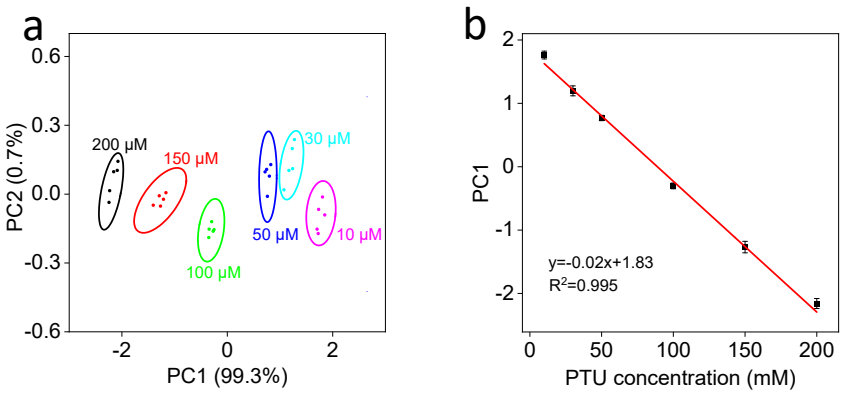

Figure S27. PCA canonical score plots and the linear calibration plots for discrimination of different concentrations of PTU.

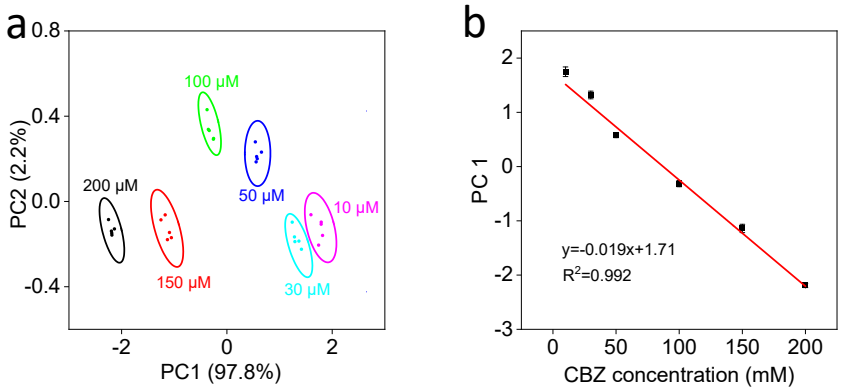

Figure S28. PCA canonical score plots and the linear calibration plots for the discrimination of different concentrations of CBZ.

3. Supplementary Tables

Table S1. Kinetic parameters of nanozymes with POD-like activity at different H_2O_2 concentrations.

Nanozyme	Substrate	K_m (mM)	V_{max} ($\times 10^{-7}$ M s^{-1})
NC	H_2O_2	36.60 ± 6.87	2.21 ± 0.181
Pt_{NP}/C	H_2O_2	58.79 ± 1.58	3.95 ± 0.607
Pt_{NP}/NC	H_2O_2	16.95 ± 1.15	5.28 ± 0.744